PERIODICO di MINERALOGIA
established in 1930

DIPARTIMENTO DI SCIENZE DELLA TERRA
SAPIENZA UNIVERSITÀ DI ROMA

An International Journal of
Mineralogy, Crystallography, Geochemistry,
Ore Deposits, Petrology, Volcanology
and applied topics on Environment, Archaeometry and Cultural Heritage

Micro-Raman spectroscopy of selected Mo minerals from Su Seinargiu (Sardinia, Italy)

Daniela Mauro *, Cristian Biagioni, Paolo Orlandi

Department of Earth Sciences, University of Pisa, Via Santa Maria 53, 56126 Pisa, Italy

ARTICLE INFO

Submitted: July 2020
Accepted: November 2020
Available on line: January 2021

* Corresponding author:
daniela.mauro@dst.unipi.it

Doi: 10.13133/2239-1002/16940

How to cite this article:
Mauro D. et al. (2021)
Period. Mineral. 90, 229-237

ABSTRACT

Raman spectra of selected molybdenum minerals, represented both by bismuth-molybdenum oxides (sardignaite, gelosaite, and mambertiite) and by molybdates [tancaite-(Ce), ichnusaite, nuragheite, and suseinargiuite] from the Su Seinargiu Mo-Bi prospect (Sardinia, Italy) are reported. Raman spectra were collected using samples previously characterized through X-ray diffraction and electron-microprobe analyses. Bismuth-molybdenum oxides are mainly characterized by bands in the range between 300 and 1000 cm^{-1}, related to stretching modes of Mo–O and to Bi–O bonds. Bands related to O–H stretching modes were observed in the range between 3000 and 4000 cm^{-1}. Raman spectra of molybdates are characterized by the four fundamental modes of MoO_4 groups occurring between 250 and 1000 cm^{-1}. Additionally, stretching bands related to O–H bonds were observed in tancaite-(Ce). Micro-Raman spectroscopy is an efficient tool for the discrimination of these rare phases, with some exceptions discussed in the text.

Keywords: bismuth-molybdenum oxides; molybdates; micro-Raman spectroscopy; Su Seinargiu; Italy.

INTRODUCTION

Molybdenum (Z=42) is a relatively rare element, having a continental crustal abundance of 1.1 µg/g (e.g., Wedepohl, 1995). It is the constituent of 70 minerals currently accepted by the IMA-CNMNC and occurs, in natural and synthetic compounds, in several oxidation states, from -4 to +6.

One of the most important localities for the study of Mo mineralogy is likely the small Su Seinargiu prospect, Sardinia, Italy. There, more than 50 different mineral species have been identified and most of them are alteration products of a primary molybdenite ±bismuthinite±bismuth assemblage (Orlandi et al., 2013). Among them, thirteen are secondary Mo minerals and seven were discovered for the first time from this Italian locality, justifying the role of Su Seinargiu as a reference locality for the study of Mo mineralogy. The seven new mineral species are represented by bismuth-molybdenum oxides (sardignaite, gelosaite, and mambertiite) and by molybdates [tancaite-(Ce), ichnusaite, nuragheite, and suseinargiuite] (Orlandi et al., 2010, 2011, 2014, 2015a, 2015b, 2015c; Bonaccorsi and Orlandi, 2020).

Molybdates and bismuth-molybdenum oxides are studied for their properties and potential applications in the field of catalysis, photocatalysis, and luminescence (Ait ahsaine et al., 2016). Indeed, bismuth-molybdenum oxides and molybdates are used in the production of lithium batteries, scintillation detectors, humidity sensors, and microwave dielectric devices (Chae et al., 2003). In addition actinide molybdates have been reported as alteration products of spent nuclear fuel (Xiao et al., 2016) under repository conditions similar to those proposed for Yucca Mountain, Nevada (U.S.A.), playing a role in the storage and release of actinides in the environment. Raman spectroscopy has been recognised as a useful tool to identify quickly and in a not-destructive way the molybdenum synthetic products

(Crane et al., 2002). Consequently, the aim of this paper is to contribute to the knowledge of Mo compounds, reporting and briefly discussing the Raman spectra of well-characterized specimens of the rare Mo minerals found at the Su Seinargiu prospect.

EXPERIMENTAL

The studied specimens are represented by the type material of the new mineral species described from Su Seinargiu and kept in the mineralogical collection of the Museo di Storia Naturale of the Università di Pisa, Via Roma 79, Calci, Pisa, Italy.

Micro-Raman spectra of these phases were collected using both polished or unpolished samples, in nearly back-scattered geometry, on unoriented grains, using a Horiba Jobin-Yvon XploRA Plus apparatus, equipped with a motorized *x*-*y* stage and an Olympus BX41 microscope with a 50× objective, the only exception being represented by suseinargiuite, for which a 100× objective was used. Raman spectra were excited using a 532 nm line of a solid-state laser, attenuated to 10% (i.e., 2.5 mW) to avoid any potential damage to these phases owing to their uniqueness and extreme rarity. In this way, no damage was observed. The minimum lateral and depth resolution was set to a few μm. The system was calibrated using the 520.6 cm^{-1} Raman band of silicon before each experimental session. Spectra were collected through multiple acquisitions (3) with variable counting times, ranging from 60 to 120 s. Backscattered radiation was analyzed with a 1200 gr/mm grating monochromator. Raman spectra were processed using *Fityk* (Wojdyr, 2010), subtracting the background and fitting the spectra to theoretical peak shapes using Voigt functions. Experimental precision can be estimated at ±2 cm^{-1}. In the following, a brief description of the studied samples and their crystal structure are reported.

Sardignaite

Sardignaite is monoclinic, space group $P2_1/m$, with unit-cell parameters a=5.7797(7), b=11.567(1), c= 6.3344(8) Å, β=113.360(9)°, V=388.8(1) $Å^3$. The empirical formula of sardignaite is $Bi_{0.980}Pb_{0.010}Mo_{2.007}O_7(OH)_{1.000}\cdot 2H_2O$, ideally $BiMo_2O_7(OH)\cdot 2H_2O$ (Orlandi et al., 2010). It occurs as pale yellow or bluish {001} tabular crystals, up to 1 mm long. The crystal structure is composed by zig-zag chains formed by corner-sharing Mo-centred octahedra, with Bi polyhedra between the octahedral chains (Figure 1a). Holotype specimen (catalogue number 19350), represented by a yellow tabular crystal, was used for data collection.

Gelosaite

Gelosaite is monoclinic, space group $P2_1/n$. The studied sample (holotype material, catalogue number 18910), represented by the pale blue crystal studied by Orlandi et al. (2011), has unit-cell parameters a=5.8570(5), b=9.0517(8), c=13.992(1) Å, β=100.44(1)°, V=729.5(1) $Å^3$. The empirical formula of gelosaite is $Bi_{1.03}Mo^{6+}_{1.47}Mo^{5+}_{0.62}H_{3.01}O_9$, ideally $BiMo_2O_7(OH)\cdot H_2O$ (Orlandi et al., 2011). It occurs as colourless to pale blue to yellow transparent {100} tabular crystals, elongated on [010], up to 1 mm in length. Its crystal structure is formed by two kinds of layers. The first one is formed by distorted MoO_6 octahedra, forming edge-sharing zig-zag chains, with an additional partially occupied Mo-centred site; the other layer is composed by Bi-centred eight-fold coordinated polyhedra, forming dimers, with an additional partially occupied Mo-centred position (Figure 1b).

Mambertiite

Mambertiite is triclinic, space group P-1, with unit-cell parameters a=5.854(2), b=9.050(3), c=7.637(3) Å, α=112.85(1), β=102.58(1), γ=90.04(1)°, V=362.3(2) $Å^3$. The empirical formula is $Bi_{0.99}(Mo^{5+}_{2.74}W_{0.05})O_{7.97}(OH)_{1.03}$, ideally $BiMo^{5+}_{2.80}O_8(OH)$ (Orlandi et al., 2015a). It occurs as pale yellow {001} tabular individuals, up to 1 mm long. The crystal structure is formed by zig-zag chains formed by edge-sharing Mo-centred octahedra, with Bi dimers between the octahedral chains (Figure 1c). Mambertiite has a Mo content higher than that shown by gelosaite and a different stacking sequence of their constitutive layers. Indeed, these two species could indicate the occurrence of order-disorder phenomena within the gelosaite-mambertiite series. Raman data were collected on holotype material, catalogue number 19682.

Tancaite-(Ce)

Tancaite-(Ce) has a cubic sub-cell, space group Pm-3m, with unit-cell parameter a=6.870(1) Å; its actual symmetry is likely lower [maybe trigonal, space group R-3, with unit-cell parameters a=19.2901(3), c=47.2510(5) Å]. Its empirical formula is $Fe^{3+}_{1.03}(Ce_{0.46}La_{0.23}Nd_{0.16}Pr_{0.05}Sm_{0.01}U_{0.01}Th_{0.07})(Mo_{2.96}Si_{0.04})O_{12}\cdot 3H_2O$, ideally $Fe^{3+}Ce(MoO_4)_3\cdot 3H_2O$ (Bonaccorsi and Orlandi, 2020). It forms pseudo-cubic and pseudo-octahedral red or pale-brown individuals, up to 1 mm in size. Only the "average" crystal structure was solved, showing Fe-centred octahedra connected, through corner-sharing, with statistically occupied Mo-centred tetrahedra. Cerium is hosted in 6+3 polyhedra (Figure 2a), being coordinated by six oxygen atoms and three H_2O groups (Bonaccorsi and Orlandi, 2020). The studied sample is represented by the holotype material of tancaite-(Ce) (catalogue number 18911), formed by a pseudo-cubic brown crystal, *ca*. 1 mm in size.

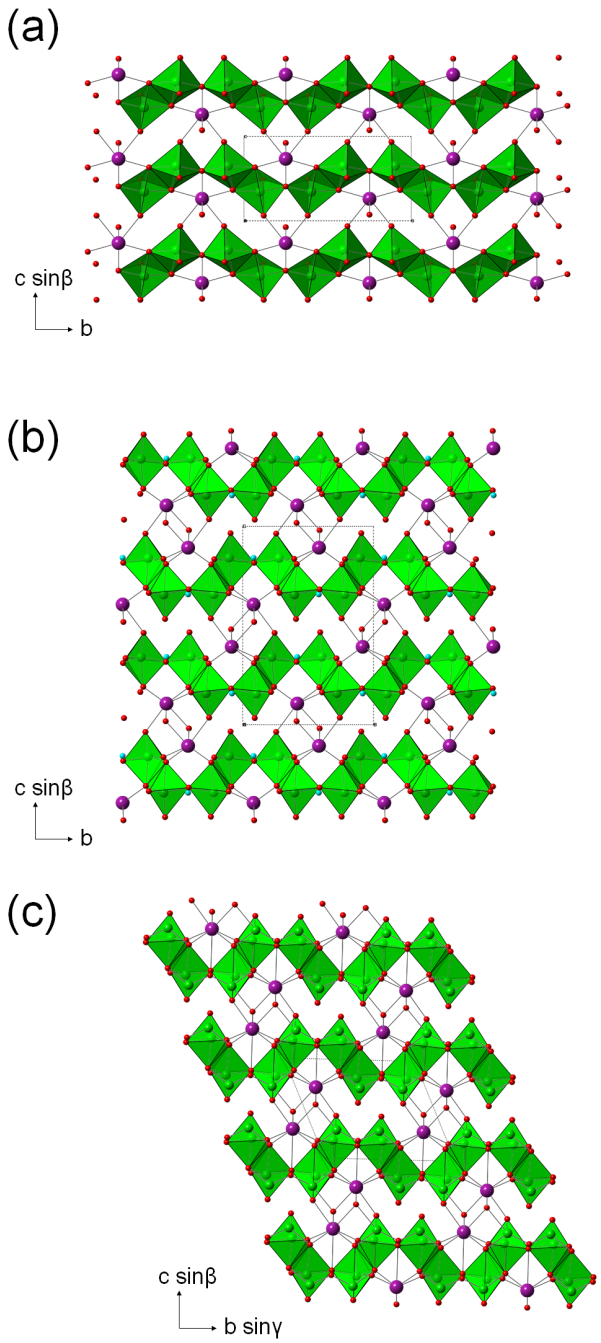

Figure 1. Projections of the crystal structures of the bismuth-molybdenum oxides sardignaite (a), gelosaite (b), and mambertiite (c). Mo-centred polyhedra are shown as green octahedra, whereas Bi and O atoms are shown as violet and red circles, respectively; H_2O groups are shown as light blue circles.

Suseinargiuite

Suseinargiuite is tetragonal, space group $I4_1/a$, with unit-cell parameters a=5.296(1), c=11.673(2) Å, V=327.4(1) Å^3. It occurs as hemispherical aggregates (up to 0.2-0.3 mm in diameter) of colourless acicular crystals, up to few µm in size. Suseinargiuite is the analogue of synthetic $(Na_{0.5}Bi_{0.5})MoO_4$ (e.g., Hanuza et al., 1997) and it has a scheelite-type structure, with Na^+ and Bi^{3+} randomly distributed at the eight-fold coordinated site, whereas Mo is tetrahedrally coordinated (Figure 2b). Holotype material (catalogue number 19692) is represented by the polished hemispherical aggregate described in Orlandi et al. (2015c); it is chemically zoned, with two domains having empirical formula $(Na_{0.35}Bi_{0.54}Pb_{0.04})Mo_{0.99}O_4$ and $(Na_{0.31}Bi_{0.46}Pb_{0.17})Mo_{0.99}O_4$, ideally $(Na_{0.5}Bi_{0.5})MoO_4$ (Orlandi et al., 2015c).

Ichnusaite

Ichnusaite, is monoclinic, space group $P2_1/c$, with unit-cell parameters a=9.6797(12), b=10.3771(13), c=9.3782(12) Å, β=90.00(1)°, V=942.0(2) Å^3. The empirical formula, $Th_{0.99}Mo_{2.01}O_8 \cdot 3H_2O$, agrees with the ideal one, $Th(MoO_4)_2 \cdot 3H_2O$ (Orlandi et al., 2014). It occurs as aggregates of colourless {100} tabular individuals, up to 200 µm in length. The crystal structure is formed by layers of nine-fold coordinated Th-centred polyhedra and Mo-centred tetrahedra. Among the three H_2O groups occurring in its crystal structure, two are directly bonded to the Th-centred polyhedra whereas the third occurs in the interlayer and is bonded to successive layers through hydrogen bonds only (Figure 2c). The studied sample (a lozenge-shaped crystal, *ca*. 0.2 mm in size) is represented by the holotype material (catalogue number 19679).

Nuragheite

Nuragheite is monoclinic, space group $P2_1/c$, with unit-cell parameters a=7.358(2), b=10.544(3), c=9.489(2) Å, β=91.88(2)°, V=735.8(2) Å^3. The empirical formula, $Th_{1.00}Mo_{2.00}O_8 \cdot H_2O$, is in agreement with the ideal one, $Th(MoO_4)_2 \cdot H_2O$ (Orlandi et al., 2015b). It occurs as aggregates of colourless {100} tabular crystals, up to 200 µm long. The crystal structure is formed by heteropolyhedral layers topologically identical to that occurring in ichnusaite. However, nuragheite contains only one H_2O group directly bonded to Th-centred polyhedra. Successive layers are held together through the sharing of oxygen atoms between Th-centred polyhedra and Mo-centred tetrahedra (Figure 2d). Holotype material of nuragheite (catalogue number 19680) was used for data collection.

RESULTS AND DISCUSSION

Tables 1 and 2 give the observed Raman bands and their interpretation. The band positions were found through profile fitting using Fityk (Wojdyr, 2010). In the following, the Raman features characterizing the studied phases are briefly discussed.

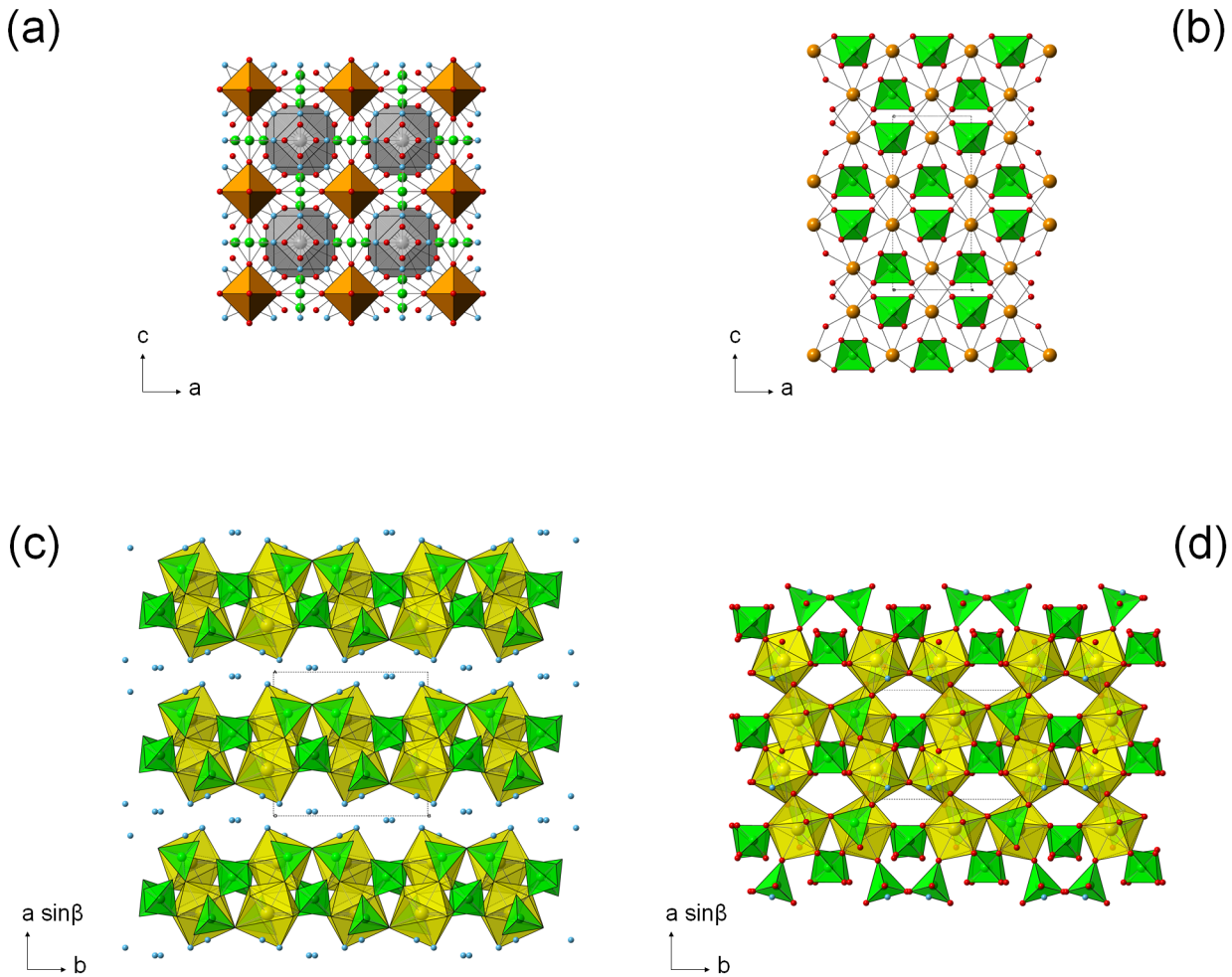

Figure 2. Projections of the crystal structures of the molybdates tancaite-(Ce) (a), suseinargiuite (b), ichnusaite (c), and nuragheite (d). In (a), Fe-centred octahedra and Ce-centred polyhedra are shown as dark orange and light-grey polyhedra, respectively. Molybdenum, O and H_2O groups are shown as green, red and light blue circles, respectively. In (b), Mo-centred tetrahedra are shown in green, whereas the (Na/Bi) and O atoms are shown as orange and red circles, respectively. In (c) and (d), the Mo-centred tetrahedra are green, whereas Th-centred polyhedra are yellow. H_2O groups and O atoms are shown as light blue and red circles, respectively.

Sardignaite

The Raman spectrum of sardignaite, in the range between 100 and 1100 cm^{-1}, is shown in Figure 3a. It can be divided into three regions, i.e., between (i) 750-1100 cm^{-1}, (ii) 300-750 cm^{-1}, and (iii) 100-300 cm^{-1}. In agreement with Hardcastle and Wachs (1991), the two strong Raman bands at 859 and 912 cm^{-1} occurring in the region (i) may be attributed to the shortest Mo–O bonds whereas the weak bands occurring in the second range (ii) are likely related to longer Mo–O bonds as well as to Bi–O bonds. The interpretation of the Raman bands in the third range (iii) is not straightforward, owing to the possible overlap of the bending modes of Mo–O and Bi–O bonds as well as the lattice vibration modes. Stretching modes of H_2O and OH groups are represented by a weak and broad band in the region between 3000 and 4000 cm^{-1} (Figure 3b). Its deconvolution revealed the occurrence of five components (Table 1). No bending mode related to the H–O–H bonds of the H_2O groups was observed in the studied sample.

In addition, Raman spectra were collected on a bluish tabular crystal (not belonging to the type material), identified also through X-ray diffraction; this sample showed the same spectral features of holotype material.

Gelosaite and mambertiite

The crystal structures of gelosaite and mambertiite are characterized by the same kind of zig-zag layers and differ only for the different stacking sequence of their constitutive layers and for the higher content of Mo shown by mambertiite, coupled with the lower amount

Table 1. Raman bands (cm^{-1}) and band assignments of bismuth-molybdenum oxides.

Sardignaite	Gelosaite	Mambertiite	Assignments
133, 145, 180, 219, 313, 342, 366	132, 153, 164, 198, 215, 233, 262, 269, 296, 347, 364, 396	119, 136, 160, 194, 210, 217, 223, 241, 257, 273, 290, 298, 361	Mo–O, Bi–O and lattice modes
410, **516**, 643	439, **521**, 637, 676	418, 449, **519**, **635**, 667	Mo–O and Bi–O modes
846, **859**, **912**	**847**, 886, **900**, 938, **940**	**844**, 866, **896**, 930, **938**	Mo–O modes
-	1613	-	ν_2 (H_2O)
3067, 3210, 3331, 3461, 3485	3320, 3406, 3466, 3514	3315, 3468	O–H stretching modes

The strongest Raman bands are shown in bold.

Table 2. Raman bands (cm^{-1}) and band assignments of molybdates.

Tancaite-(Ce)	Suseinargiuite	Ichnusaite	Nuragheite	Assignments
-	126, 183, 282, 302	113, 152, 165, 174, 212	-	*M*–O and lattice modes
287, 333, 349, 426	319, 326, 368, 406	266, 280, 301, 317, 332, 340, 355, 377	274, 318, 350, 381	$\nu_2 + \nu_4$ (MoO_4)
744, **809**, 855	773, 790,	**778**, 797, 820, 832	**779, 798**, 829	ν_3 (MoO_4)
934, 951	862, **875**, 895, 910	910, 921, 934, **943**, 949	930, **943**, 951	ν_1 (MoO_4)
3233, 3445, 3682	-	-	-	O–H stretching modes

The strongest Raman bands are shown in bold.

of H_2O shown by the latter (having only one OH group) with respect to gelosaite, having both OH and H_2O groups (Orlandi et al., 2011, 2015b). This is likely the reason for the very similar Raman spectra shown by these two phases (Figure 3 c-f), particularly in the region between 100 and 1100 cm^{-1} (Figure 3 c,e).

The Raman spectra of gelosaite and mambertiite are both characterized by the occurrence of three strong bands between 800 and 1000 cm^{-1} (Table 1; Figure 3 c,e). These strong bands are likely related to the stretching modes of the shortest Mo–O bonds (e.g., Hardcastle and Wachs, 1991). Other weaker bands occur between 300 and 800 cm^{-1} and are likely related to longer Mo–O bonds and to Bi–O bonds. The low wavenumber region (<300 cm^{-1}) is characterized by weak bands that can be attributed to Mo–O, Bi–O, and lattice modes. Some peculiarities can be recognized in the O–H stretching and bending regions of these two minerals. Indeed, four bands at 3320, 3406, 3466, and 3514 cm^{-1} (Figure 3d) and a weak band at 1613 cm^{-1} can be observed in the Raman spectrum of gelosaite, agreeing not only with the occurrence of OH groups, but also with the presence of H_2O. The Raman spectrum of mambertiite, in the region between 3000 and 4000 cm^{-1}, is noisy and it allows the identification of only two bands at 3315 and 3468 cm^{-1} (Figure 3f).

Tancaite-(Ce)

The Raman spectrum of tancaite-(Ce), in the region between 100 and 1100 cm^{-1}, is reported in Figure 4a. In agreement with Bonaccorsi and Orlandi (2020), it shows Raman bands in the range between 700-1000 cm^{-1} and between 250 and 450 cm^{-1} related to the symmetric and antisymmetric stretching (ν_1 and ν_3) vibrations as well as to bending modes (ν_2 and ν_4) of the MoO_4 groups. The occurrence of multiple bands related to Mo–O bonds suggests the presence of structurally different MoO_4 groups, agreeing with the structural complexity suggested by Bonaccorsi and Orlandi (2020). The strongest Raman bands occur at 809 and 951 cm^{-1} and can be interpreted as due to the ν_3 and ν_1 modes of MoO_4 groups, respectively. Their positions agree with those reported by Bonaccorsi and Orlandi (2020), i.e., 812 and 955 cm^{-1}. The band at 809 cm^{-1} has two shoulders at higher and lower wavenumbers, *i.e.*, 744 and 855 cm^{-1}, respectively. In addition, the band at 951 cm^{-1} has an asymmetry towards lower wavenumbers; its deconvolution suggests the occurrence of two components, at 934 and 951 cm^{-1}. Similar Raman bands were reported by Bonaccorsi and Orlandi (2020) at 743, 863, and 927 cm^{-1}, respectively. In the low wavenumber region, a complex band centred at 349 cm^{-1} has contribution from two other weaker bands at 287 and

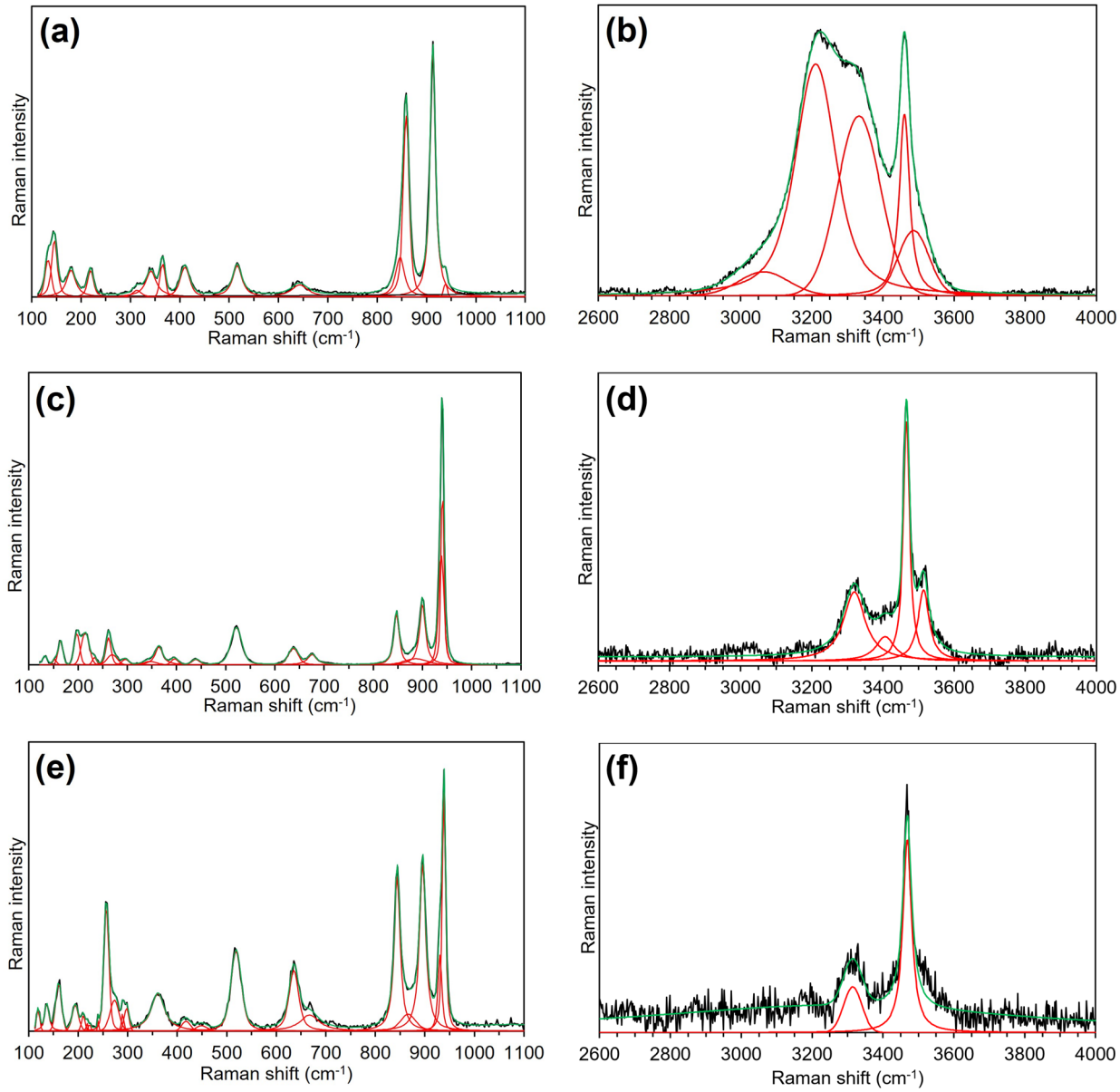

Figure 3. Raman spectra of bismuth-molybdenum oxides in the regions 100-1100 cm^{-1} and 2600-4000 cm^{-1}: (a) and (b) sardignaite; (c) and (d) gelosaite; (e) and (f) mambertiite. The cumulative curves are shown in green whereas fitted bands are in red.

333 cm^{-1}. An additional weak band occurs at 426 cm^{-1}. The following bands were reported by Bonaccorsi and Orlandi (2020) in the same spectral region: 297, 354, and 432 cm^{-1}. The disagreement between our study and those reported by the latter authors it is likely due to the fact that these authors established the peak positions using a basic peak-finding routine. The hydrated nature of tancaite-(Ce) is confirmed by the occurrence of O–H stretching modes with three bands at 3233, 3445 and 3682 cm^{-1} in the O–H stretching region (Figure 5). A broad and weak band occur in the bending region of O–H bonds. Finally, Bonaccorsi and Orlandi (2020) reported the occurrence of bending and stretching vibrations related to O–H bonds at 1620 and 3430 cm^{-1}, respectively.

Suseinargiuite

The Raman spectrum of suseinargiuite in the range between 100 and 1100 cm^{-1} was previously reported (Orlandi et al., 2015c) and it was compared with that of synthetic $(Na_{0.5}Bi_{0.5})MoO_4$ (Hanuza et al., 1997). Suseinargiuite has isotypic relations with wulfenite, $PbMoO_4$, from which it can be derived through the coupled heterovalent

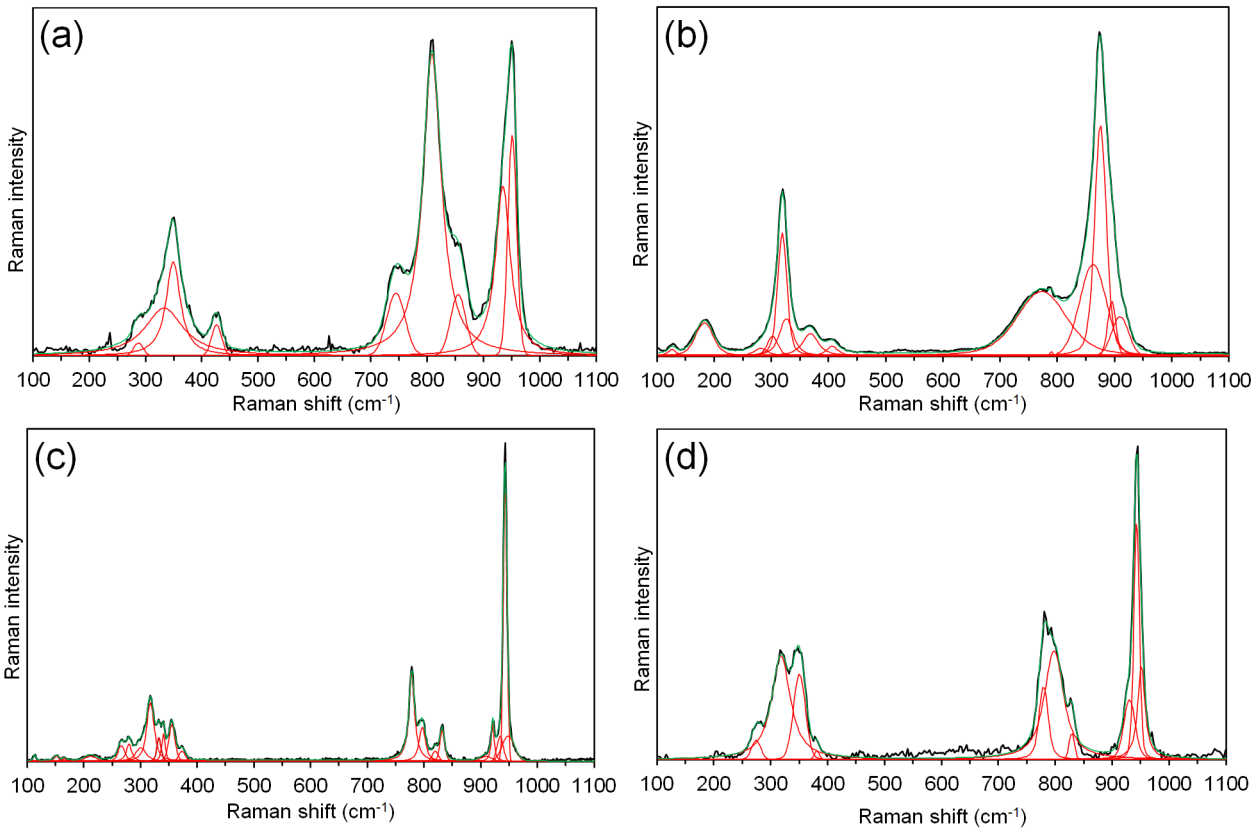

Figure 4. Raman spectra of molybdates in the range 100-1100 cm^{-1}: (a) tancaite-(Ce), (b) suseinargiuite, (c) ichnusaite, and (d) nuragheite. The cumulative curves are shown in green whereas fitted bands are in red.

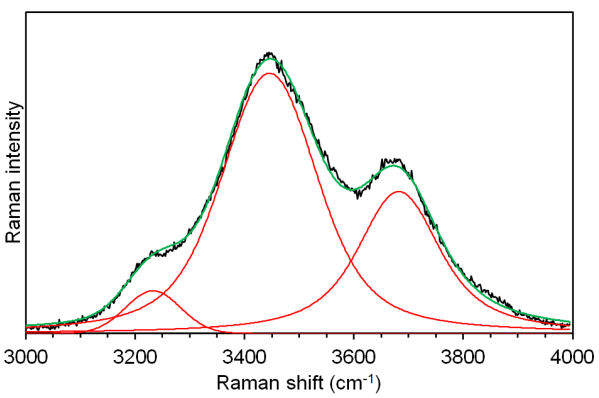

Figure 5. Raman spectra of tancaite-(Ce) in the range 3000-4000 cm^{-1}. The cumulative curve is shown in green whereas fitted bands are in red.

substitution $Pb^{2+}=Na^{+}_{0.5}+Bi^{3+}_{0.5}$. As a consequence of this structural relation, the Raman spectrum of suseinargiuite is very similar to that of wulfenite (Crane et al., 2002) and it is characterized by features related to stretching and bending modes of the MoO_4 groups. (Figure 4b). The strong and broad band at 875 cm^{-1} is interpreted as the v_1 mode of the MoO_4 group. This Raman band can be compared with those previously reported by Orlandi et al. (2015c) and Hanuza et al. (1997), i.e., 876 cm^{-1}. Actually, this band has several components at 862, 875, 895, and 910 cm^{-1}. A broad shoulder centered at 773 cm^{-1} may be interpreted as due to the v_3 mode of MoO_4 groups, in agreement with Hanuza et al. (1997). The bands in the range ~300-400 cm^{-1} are attributed to the v_2+v_4 bending modes whereas the two bands at 183 and 126 cm^{-1} are interpreted as the vibration of the metal-oxygen bonds and/or to the lattice modes. The anhydrous nature of suseinargiuite is confirmed by the absence of spectral features in the region between 3000 and 4000 cm^{-1}.

Ichnusaite and nuragheite

Ichnusaite and nuragheite are characterized by the same heteropolyhedral layers, differing in the hydration state and the connection of successive layers (Orlandi et al., 2014; Orlandi et al., 2015b). Likely, these structural relationships are the reason for the strong similarity between the Raman spectra of these two minerals, showing similar spectral features in the ranges 750-950 and 350-

450 cm^{-1} (Figure 4 c,d), possibly related to stretching and bending modes of MoO_4 groups, in agreement with Xiao et al. (2014) for synthetic cesium-thorium molybdates. The occurrence of multiple bands for the MoO_4 groups agrees with the presence of two structurally different MoO_4 units. Three main regions are characterized by the occurrence of Raman bands, i.e., 900-1000 cm^{-1}, 750-850 cm^{-1}, and 250-450 cm^{-1}, corresponding to the ν_1, ν_3 and ν_2+ν_4 modes of MoO_4 groups. The occurrence of bending and stretching modes related to the O–H bonds cannot be observed on the studied samples owing to the occurrence of fluorescence phenomena.

CONCLUSION

Raman spectroscopy is a useful tool for the identification of the rare bismuth-molybdenum oxides and molybdates described from the Su Seinargiu prospect. Since Raman spectra have been collected on well-characterized samples, the reported data represent an important addition to the knowledge of these very rare phases and may help other researchers in their identification.

Sardignaite can be easily distinguished from gelosaite and mambertiite, owing to the presence of two strong bands at 859 and 912 cm^{-1}. On the contrary, the distinction of gelosaite and mambertiite using only the strongest Raman bands seems difficult because both minerals are characterized by the occurrence of three strong bands in the same spectral range, i.e., between 800 and 1000 cm^{-1}. Likely, this is a consequence of the close structural similarity between these two bismuth-molybdenum oxides. However, subtle differences can be observed in the spectral range below 800 cm^{-1}. As regards the O–H stretching region, some differences seem to occur between gelosaite and mambertiite. For instance, the former has three relatively strong bands, whereas the latter shows only two bands. This may be related to the lower hydration state of mambertiite with respect to gelosaite. However, owing to the noisy nature of the mambertiite spectrum, a confident distinction between these two minerals based on the O–H stretching region may not be possible.

Among the studied molybdates, the identification of tancaite-(Ce) is relatively easy, considering the strong band at 951 cm^{-1}. Ichnusaite and nuragheite show the strongest Raman bands at the same position, i.e., 943 cm^{-1}. However, some differences can be observed in the spectral range below 850 cm^{-1}, giving us the opportunity to identify both minerals using Raman spectroscopy only. Finally, the Raman spectrum of suseinargiuite is similar to that of wulfenite, with a strong and broad band at 875 cm^{-1}. Taking into account the possible existence of a substitutional series between suseinargiuite and wulfenite, chemical analyses are required to achieve an accurate identification.

ACKNOWLEDGEMENTS

Giorgio Bortolozzi is thanked for providing us with the specimen of blue sardignaite investigated in this study. This research was financially supported by the Ministero dell'Istruzione, Università e Ricerca through the project PRIN 2017 "TEOREM-deciphering geological processes using Terrestrial and Extraterrestrial ORE Minerals", prot. 2017AK8C32. The comments of two anonymous reviewers improved the manuscript.

REFERENCES

Ait ahsaine H., Zbair M., Ezahri M., Benlhachemi A., Bakiz B., Guinneton F.,Gavarri J-R., 2016. Structural and temperature-dependent vibrational analyses of the non-centrosymmetric $ZnMoO_4$ molybdate. Journal of Materials and Environmental Science 7, 3076-3083.

Bonaccorsi E. and Orlandi P., 2020. Tancaite-(Ce), ideally $FeCe(MoO_4)_3 \cdot 3H_2O$: description and average crystal structure. European Journal of Mineralogy 32, 347-354.

Chae B., Jung M.Y., Wu X., Kim S.B., 2003. Characterization of a series of sodium molybdate structures by two-dimensional Raman correlation analysis. Journal of Raman Spectroscopy 34, 451-458.

Crane M., Frost R.L., Williams P.A., Kloprogge J.T., 2002. Raman spectroscopy of the molybdate minerals chillagite (tungsteinian wulfenite-*I*4), stolzite, scheelite, wolframite and wulfenite. Journal of Raman Spectroscopy 33, 62-66.

Hanuza J., Haznar A., Mączka M., Pietraszko A., Lemiec A., van der Maas J.H., Lutz E.T.G., 1977. Structure and vibrational properties of tetragonal scheelite $NaBi(MoO_4)_2$. Journal of Raman Spectroscopy 28, 953-963.

Hardcastle F.D. and Wachs I.E., 1991. Molecular structure of molybdenum oxide in bismuth molybdates by Raman spectroscopy. The Journal of Physical Chemistry 95, 10763-10772.

Orlandi P., Pasero M., Bigi S., 2010. Sardignaite: a new mineral, the second known bismuth molybdate: description and crystal structure. Mineralogy and Petrology 100, 17-22.

Orlandi P., Demartin F., Pasero M., Leverett P., Williams P.A., Hibbs D.E., 2011. Gelosaite, $BiMo^{6+}_{(2-5x)}Mo^{5+}_{6x}O_7(OH)\cdot H_2O$($0 \leq x \leq 0.4$), a new mineral from Su Senargiu (CA), Sardinia, Italy, and a second occurrence from Kingsgate, New England, Australia. American Mineralogist 96, 268-273.

Orlandi P., Gelosa M., Bonacina E., Caboni F., Mamberti M., Tanca G.A., Vinci A., 2013. Sardignaite, gelosaite et tancaite-(Ce): trois nouveaux minéraux de Su Seinargiu, Sarroch, Sardaigne, Italie. Le Régne Mineral 112, 39-52.

Orlandi P., Biagioni C., Bindi L., Nestola F., 2014. Ichnusaite, $Th(MoO_4)_2 \cdot 3H_2O$, the first natural thorium molybdate: occurrence, description, and crystal structure. American Mineralogist 99, 2089-2094.

Orlandi P., Biagioni C., Pasero M., Demartin F., Campostrini

I., Merlino S., 2015a. Mambertiite, $BiMo^{5+}_{2.80}O_8(OH)$, a new mineral from Su Seinargiu, Sardinia, Italy: occurrence, crystal structure, and relationships with gelosaite. European Journal of Mineralogy 27, 405-415.

Orlandi P., Biagioni C., Bindi L., Merlino S., 2015b. Nuragheite, $Th(MoO_4)_2 \cdot H_2O$, the second natural thorium molybdate and its relationships to ichnusaite and synthetic $Th(MoO_4)_2$. American Mineralogist 100, 267-273.

Orlandi P., Biagioni C., Moëlo Y., Langlade J., Faulques E., 2015c. Suseinargiuite, $(Na_{0.5}Bi_{0.5})MoO_4$, the Na-Bi analogue of wulfenite, from Su Seinargiu, Sardinia, Italy. European Journal of Mineralogy 27, 695-699.

Wedepohl K.H., 1995. The composition of the continental crust. Geochimica et Cosmochimica Acta 59, 1217-1239.

Wojdyr M., 2010. Fityk: a general-purpose peak fitting program. Journal of Applied Crystallography 43, 1126-1128.

Xiao B., Dellen J., Schlenz H., Bosbach D., Seleimanov E.V., Alekseev E.V., 2014. Unexpected structural complexity in cesium thorium molybdates. Crystal Growth & Design 14, 2677-2684.

Xiao B., Kegler P., Gesing T.S., Robben L., Blanca-Romero A., Kowalski P.M., Li Y., Klepov V., Bosbach D., Alekseev E.V., 2016. Giant volume change and topological gaps in temperature- and pressure-induced phase transitions: experimental and computational study of $ThMo_2O_8$. Chemistry-A European Journal 22, 964-958.